Applied Physics Letters

RESEARCH ARTICLE | SEPTEMBER 25 2023

Broadband bandpass Purcell filter for circuit quantum electrodynamics

Haoxiong Yan ; Xuntao Wu ; Andrew Lingenfelter ; Yash J. Joshi ; Gustav Andersson ; Christopher R. Conner ; Ming-Han Chou ; Joel Grebel ; Jacob M. Miller ; Rhys G. Povey ; Hong Qiao ; Aashish A. Clerk ; Andrew N. Cleland

Appl. Phys. Lett. 123, 134001 (2023)
https://doi.org/10.1063/5.0161893

AIP Publishing

Applied Physics Letters ARTICLE pubs.aip.org/aip/apl

Broadband bandpass Purcell filter for circuit quantum electrodynamics

Cite as: Appl. Phys. Lett. **123**, 134001 (2023); doi: 10.1063/5.0161893
Submitted: 12 June 2023 · Accepted: 9 August 2023 ·
Published Online: 25 September 2023

View Online Export Citation CrossMark

Haoxiong Yan,[1] Xuntao Wu,[1] Andrew Lingenfelter,[1,2] Yash J. Joshi,[1] Gustav Andersson,[1] Christopher R. Conner,[1] Ming-Han Chou,[1,2] Joel Grebel,[1] Jacob M. Miller,[1,2] Rhys G. Povey,[1,2] Hong Qiao,[1] Aashish A. Clerk,[1] and Andrew N. Cleland[1,3,a)]

AFFILIATIONS

[1]Pritzker School of Molecular Engineering, University of Chicago, Chicago, Illinois 60637, USA
[2]Department of Physics, University of Chicago, Chicago, Illinois 60637, USA
[3]Argonne National Laboratory, Lemont, Illinois 60439, USA

[a)]Author to whom correspondence should be addressed: anc@uchicago.edu

ABSTRACT

In circuit quantum electrodynamics, qubits are typically measured using dispersively coupled readout resonators. Coupling between each readout resonator and its electrical environment, however, reduces the qubit lifetime via the Purcell effect. Inserting a Purcell filter counters this effect while maintaining high readout fidelity but reduces measurement bandwidth and, thus, limits multiplexing readout capacity. In this Letter, we develop and implement a multi-stage bandpass Purcell filter that yields better qubit protection while simultaneously increasing measurement bandwidth and multiplexed capacity. We report on the experimental performance of our transmission-line-based implementation of this approach, a flexible design that can easily be integrated with current scaled-up, long coherence time superconducting quantum processors.

Circuit quantum electrodynamics (QED) provides a scalable approach to quantum information processing, using Josephson-based circuits as qubits.[1] A popular way to measure the quantum state of a superconducting qubit is to probe the state-dependent frequency shift of a readout resonator dispersively coupled to the qubit.[2,3] To realize fast readout, the resonator-environment coupling must be large, so that the resonator can rapidly absorb and emit measurement photons. However, the qubit relaxation time T_1 is then limited by the resulting Purcell effect.[4] To overcome this, Purcell filters have been developed, which suppress qubit emission by engineering the electrical environment seen by the readout resonator,[5–11] using, for example, a single-pole bandpass filter.[6] This, however, limits the measurement bandwidth, thus the number of readout resonators that can be measured via a single readout line, and further is incompatible with long qubit relaxation times.[12,13] For multiplexed qubit readout, one solution is to design a separate Purcell filter for each readout resonator,[14,15] but this requires good frequency matching between the filter and readout resonator, making design and fabrication more complex. A second solution is to increase the number of bandpass filter stages, yielding a broader passband and better isolation in the filter stopband,[16,17] an approach demonstrated using, e.g., coupled $\lambda/4$ resonators,[18] stepped-impedance transmission lines,[19,20] coupled mechanical resonators,[21] and coupled LC resonators.[22,23] These multi-stage designs are all symmetric, with equally coupled input and output ports. Here, we present designs for both symmetric and asymmetric bandpass filters appropriate for circuit QED, in the asymmetric case implementing different coupling rates for the input vs output ports.[6] Using the coupled-mode picture,[16,24] we show that the readout resonator coupling point to the filter must be chosen carefully, to accommodate interference between the filter stages. We demonstrate that asymmetric filters provide better qubit protection, and that broader passbands with better protection are achieved by adding filter stages. We then experimentally implement this approach and test a simple, robust design that only uses sections of transmission lines.

We first illustrate our design flow for the bandpass filters (Fig. 1). We begin with a low-pass filter prototype,[16,17] with the circuit for a normalized Nth order low-pass filter shown in Fig. 1(a), where g_0 (g_{N+1}) is the source (load) impedance number, with the source impedance normalized to $1\,\Omega$ and the filter bandwidth normalized to $\omega_c = 1$ rad/s. For a given filter response (maximally flat, equal ripple, etc.), the g_j coefficients can be calculated using the insertion loss technique[17] and Cauer synthesis.[16,24] We list the g_j coefficients for

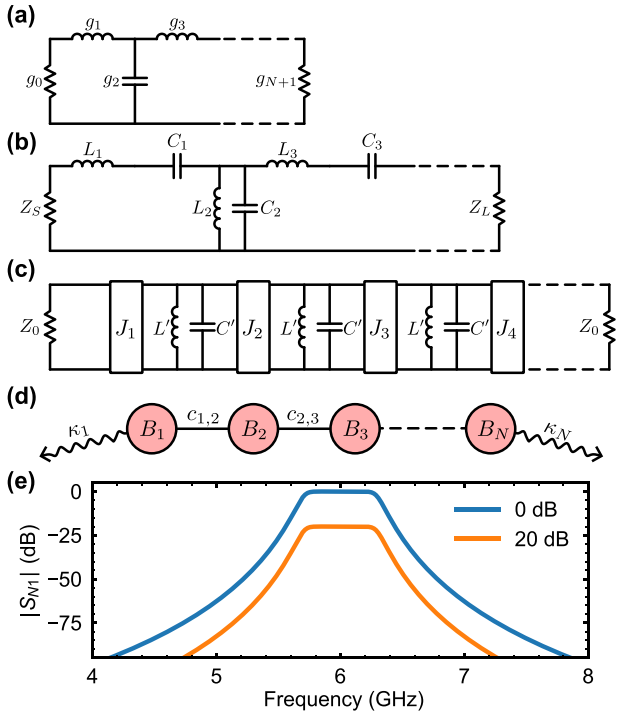

FIG. 1. Design flow for a bandpass filter. (a) Low-pass prototype, using capacitors and inductors. (b) Bandform transformation from low-pass to bandpass. (c) Bandpass filter with admittance inverters J_n, using only parallel LC resonators. (d) Coupled-mode picture for Nth order filter, with dissipation rate κ_j for the jth resonator B_j and coupling $c_{j,j+1}$ between resonators B_j and B_{j+1}. (e) Transmission coefficient $|S_{N1}|$ for 6th-order bandpass filter designs with 0 dB (blue) and 20 dB (orange) insertion loss, center frequency $\omega_0/2\pi = 6$ GHz and bandwidth $\Delta\omega/2\pi = 600$ MHz.

maximally flat, low-pass filter designs in Table I, for both conventional symmetric filters with 0 dB insertion loss and asymmetric filters with large insertion loss (20 dB). There are no lossy elements in the filter circuit, and, thus, the insertion loss comes from the reflection at the input port. A bandpass filter with large insertion loss corresponds to a filter with a weakly coupled input port and a strongly coupled output port, so that most of the driving signal reflects from the input port, while most of the signal scattered from the readout resonator is emitted from the output port, improving the readout efficiency.[6,25]

Based on the low-pass prototype in Fig. 1(a), we can obtain the bandpass filter circuit, with center frequency ω_0 and bandwidth $\Delta\omega$, through frequency and impedance scaling and bandform transformations,[16,17] as shown in Fig. 1(b). The prototype circuit contains both series and parallel LC resonators, which can be difficult to realize at microwave frequencies. We, therefore, transform this to a version with only parallel (series) LC resonators by using admittance (impedance) inverters, with an example in Fig. 1(c) using admittance inverters and identical parallel LC resonators.[17] Here, we set the source and load impedance to be $Z_0 = 50\,\Omega$, typical for circuit QED, as these circuits are typically driven and measured by 50 Ω impedance-matched electronics. Furthermore, the admittance/impedance inverters can be treated as passive couplers between the resonant LC elements,[16,24] from which we get the coupled-mode picture of a bandpass filter, as

TABLE I. Design coefficients g_j for maximally-flat low-pass filter prototypes, with $g_0 = 1$.

Insertion loss (dB)	Order	g_0g_1	g_1g_2	g_2g_3	g_3g_4	g_4g_5	g_5g_6	g_6g_7
0	1	2.000	2.000					
	2	1.414	2.000	1.414				
	3	1.000	2.000	2.000	1.000			
	4	0.765	1.414	3.414	1.414	0.765		
	5	0.618	1.000	3.236	3.236	1.000	0.618	
	6	0.518	0.732	2.732	3.732	2.732	0.732	0.518
20	1	399.0	1.003					
	2	563.6	1.003	0.708				
	3	597.5	2.003	0.668	0.500			
	4	607.6	2.417	1.709	0.415	0.383		
	5	615.2	2.621	2.344	1.237	0.277	0.309	
	6	618.3	2.734	2.734	1.868	0.911	0.196	0.259

shown in Fig. 1(d), where each red circle represents a resonator with frequency ω_0, solid lines represent the coupling $c_{j,k}$ between the jth and kth resonators, and undulating arrows represent the dissipation κ_j of the jth element; note, we assume zero intrinsic loss for all the resonators. The coupling strength and dissipation rates are given in terms of the coefficients g_j and bandwidth $\Delta\omega$ by[16,24]

$$c_{j,j+1} = \frac{\Delta\omega}{2\sqrt{g_j g_{j+1}}}, \tag{1}$$

$$\kappa_1 = \frac{\Delta\omega}{g_0 g_1}, \tag{2}$$

$$\kappa_N = \frac{\Delta\omega}{g_N g_{N+1}}. \tag{3}$$

The transmission of two example $N=6$ order bandpass filters with center frequency $\omega_0/2\pi = 6$ GHz and bandwidth $\Delta\omega/2\pi = 600$ MHz is shown in Fig. 1(e), showing flat frequency response in the bandpass as desired. From Table I, for 0 dB insertion loss, the g coefficients are symmetric and $\kappa_1 = \kappa_N$, while for 20 dB insertion loss, $\kappa_1 \ll \kappa_N$. We note that when the insertion loss goes to infinity, $g_j g_{j+1}$ $(j \geq 1)$ saturates, while $\kappa_1 = \Delta\omega/g_0 g_1$ goes to zero, approaching the singly terminated filter limit (see the supplementary material). The single-pole bandpass filter introduced in Ref. 6 can be treated as an $N=1$ bandpass filter with large insertion loss. Similar techniques have been used to design broadband Josephson parametric amplifiers[26–29] and circulators.[30,31] We will label the port coupled to the first (last) filter stage as the input (output) port, where the output port is always strongly coupled to the environment to maximize the collection of photons emitted from the readout resonator.

To realize qubit measurement, a qubit's readout resonator needs to be coupled to the filter. To better understand the differences between stages in the filter, thus where to connect the readout resonator, we calculate the local density of states (LDOS) $\rho_j(\omega)$ at the jth filter stage. When the readout resonator is coupled to the jth filter stage, its dissipation rate κ_r is proportional to the jth stage LDOS at ω_r: $\kappa_r \propto \rho_j(\omega_r)$. Assuming the qubit frequency ω_q is in the stopband, the

ratio $\rho_j(\omega_r)/\rho_j(\omega_q)$ quantifies how well the qubit is protected. The connection between the LDOS and classical circuit impedance is explained in the supplementary material. The LDOS is given by the diagonal elements of the imaginary part of the retarded Green's function $G^R_{jk}(\omega)$,[32,33]

$$G^R_{jk}(\omega) = \int \mathrm{d}t\, e^{i\omega t} G^R_{jk}(t) = -i \int \mathrm{d}t\, e^{i\omega t}\theta(t)\left\langle \left[\hat{a}_j(t), \hat{a}^\dagger_k(0)\right]\right\rangle, \quad (4)$$

$$\rho_j(\omega) = -\frac{1}{\pi}\mathrm{Im}\, G^R_{jj}(\omega), \quad (5)$$

where $\hat{a}^\dagger_j(t)$ $[\hat{a}_j(t)]$ is the creation (annihilation) operator of an excitation in the jth filter stage in the Heisenberg picture, $\theta(t)$ is the Heaviside step function, and $\langle\cdot\rangle$ is the ground state expectation value. The retarded Green's function $G^R_{jk}(\omega)$ measures the response of mode j to a probe signal of frequency ω applied to mode k, with the imaginary part yielding the linear response susceptibility; the diagonal elements $\mathrm{Im}\, G^R_{jj}(\omega)$ thus describe the susceptibility of mode j to a signal of frequency ω impinging on it, and thus how easily a resonator of frequency ω will decay when coupled to that mode. While $G^R_{jk}(\omega)$ is just a linear response susceptibility[34] and thus can be derived from classical coupled-mode theory, we choose the quantum formalism here because the filter will ultimately couple to a qubit. The quantum theory directly connects to Fermi's golden rule, enabling direct calculation of qubit decay rates[34] (see the supplementary material).

The calculated LDOSs for $N = 6$ bandpass filters with 0 and 20 dB insertion loss are shown in Fig. 2. We can see that for the 20 dB insertion loss filter, $\rho_1(\omega)$ is flat in the passband, and there are $j - 1$ near-zero points in $\rho_j(\omega)$. When the readout resonator is coupled to the jth filter stage and its frequency is close to these near-zero points, it barely decays and cannot be used to do qubit readout (see the supplementary material). We see similar features in larger insertion loss filters, which are caused by interference between different filter stages. For a symmetric filter, $\rho_j(\omega_q)$ is smallest when the readout resonator is coupled to either middle stage $j = 3$ or 4, meaning a qubit is better protected when its readout resonator is coupled to this point. In the following discussion, we will couple the readout resonators to the middle (first) stage of the symmetric 0 dB (asymmetric 20 dB) insertion loss filter.

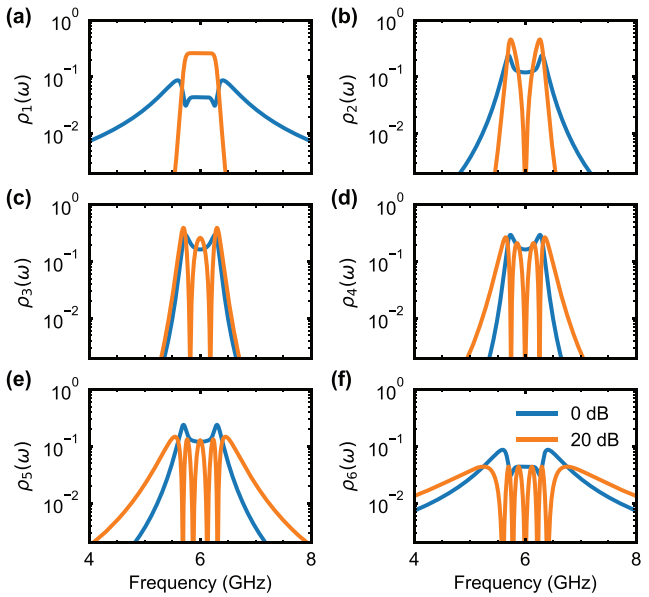

FIG. 2. (a)–(f) Local density of states (LDOS) $\rho_j(\omega)$ for the filter stages $j = 1$–6 for $N = 6$ order bandpass filters with 0 dB (blue) and 20 dB (orange) insertion loss. Bandpass filter center frequency $\omega_0/2\pi = 6$ GHz and bandwidth $\Delta\omega/2\pi = 600$ MHz. We display the LDOS for $N = 2$–5 order filters in the supplementary material.

The coupled-mode picture of the qubit readout circuit is shown in Fig. 3(a), where $c_{q,r}$ is the qubit-readout resonator coupling strength and $c_{j,r}$ is the coupling strength between the readout resonator and the jth filter stage. The qubit can decay through the readout resonator and bandpass filter modes to the input (characterized by $\kappa_{q,in}$) and output ports (characterized by $\kappa_{q,out}$). When there is no Purcell filter, the qubit lifetime $T_{1,\mathrm{bare}}$ will be limited as in Ref. 4,

$$T_{1,\mathrm{bare}} = \frac{\Delta^2_{q,r}}{\kappa_r c^2_{q,r}}, \quad (6)$$

where κ_r is the readout resonator dissipation rate and $\Delta_{q,r} = \omega_q - \omega_r$ is the frequency detuning between the qubit and readout resonator. For $\kappa_r/2\pi = 15$ MHz $(\kappa_r^{-1} \simeq 10$ ns), $\Delta_{q,r}/2\pi = -1$ GHz $(\omega_q/2\pi = 5$ GHz), and $c_{q,r}/2\pi = 100$ MHz, the qubit relaxation time T_1 is limited to 1 μs. To quantify the protection from the bandpass filter, we display the qubit lifetime T_1 vs qubit-resonator detuning $\Delta_{q,r}$ with the filter as shown in Fig. 3(b), where we treat the transmon qubit as a

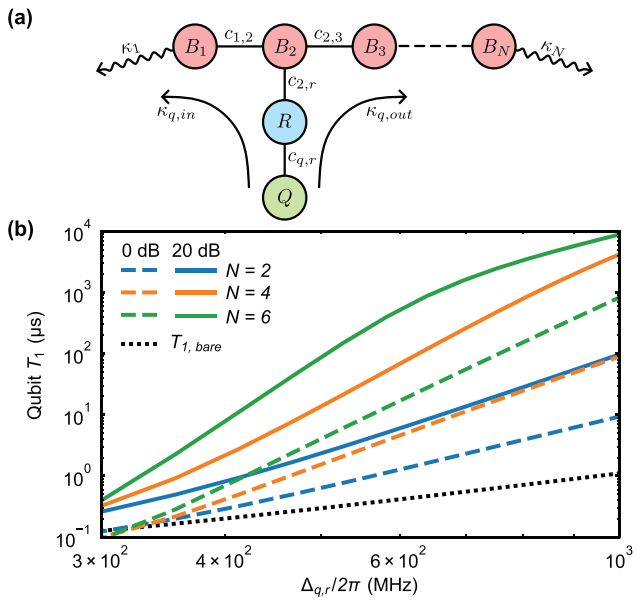

FIG. 3. (a) Coupled-mode picture of dispersive readout circuit, with qubit Q coupled through readout resonator R to filter element B_j. (b) Qubit lifetime T_1 vs qubit-resonator detuning $\Delta_{q,r}$ for bandpass filters with 0 dB (dashed lines) and 20 dB (solid lines) insertion loss. The filter center frequency $\omega_0/2\pi$ is 6 GHz, its bandwidth $\Delta\omega/2\pi$ is 600 MHz, the readout resonator frequency $\omega_r/2\pi$ is 6 GHz, the readout resonator dissipation rate $\kappa_r/2\pi$ is 15 MHz, and the qubit-resonator coupling $c_{q,r}/2\pi$ is 100 MHz.

resonator and use the classical coupled-resonator model to extract the qubit T_1. Adding more stages and using larger qubit-resonator detuning gives longer qubit lifetime. Comparing a 0 dB with a 20 dB insertion loss filter, the higher insertion loss filter affords better protection. Note that for a large insertion loss filter, $\kappa_1 \ll \kappa_N$, so the qubit mainly decays through the output port ($\kappa_{q,in} \ll \kappa_{q,out}$). We find that for symmetric filters (0 dB insertion loss) with order $N = 2k$ or $N = 2k - 1$, the qubit lifetime T_1 scales as $T_1 \propto \Delta_{q,r}^{2k+2}$. For asymmetric filters (large insertion loss) with order N, the qubit lifetime scales as $T_1 \propto \Delta_{q,r}^{2N+2}$, consistent with the single-pole bandpass filter[6] $T_1 \propto \Delta_{q,r}^{4}$. When increasing the number of stages, the qubit T_1 is lower than power-law scaling for the 20 dB insertion loss filter when the qubit-resonator detuning is large, due to the finite κ_1 as here the readout resonator is coupled to the first stage. If we further increase the insertion loss, or simply reduce κ_1, the qubit T_1 will be closer to power-law scaling (see the supplementary material). Here, we demonstrate that by adding additional stages to the bandpass filter, we can achieve better qubit protection.

In Fig. 4(a), we display a simpler bandpass filter design, using transmission line resonators in place of lumped L and C elements, which can be more easily implemented in a thin-film planar geometry. We use shorted-to-ground transmission line elements to act as the impedance (K) inverters,[17] where we adjust the length ℓ_n of each line in Fig. 4(a) according to

$$\phi_n = \arctan\left(\frac{Z_0/K_n}{1-(Z_0/K_n)^2}\right), \tag{7}$$

$$\theta_n = \pi - \arctan(Z_0/K_n) - \arctan(Z_0/K_{n+1}), \tag{8}$$

where ϕ_n and θ_n represent $\beta\ell_n$ with β the phase constant at frequency ω_0, and K_n, the impedance inverter values, respectively, satisfy

$$Z_0/K_n = \sqrt{\frac{\pi\Delta\omega}{2\omega_0 g_{n-1} g_n}} \quad \text{for } n = 1, N+1, \tag{9}$$

$$Z_0/K_n = \frac{\pi\Delta\omega}{2\omega_0\sqrt{g_{n-1}g_n}} \quad \text{for } n = 2, \ldots, N. \tag{10}$$

The figure shows a single qubit readout, where a quarter-wavelength transmission line resonator (blue) acts as the readout resonator, inductively coupled to the second bandpass filter stage and capacitively coupled to an Xmon qubit[3,35] (green). More qubits can be read out by attaching them to the same or other filter stages; to couple more readout resonators to one filter stage, a $n\lambda/2$ transmission line resonator can be used.

The single-stage ($N = 1$) asymmetric version of this circuit has been demonstrated in Refs. 36 and 37. Compared to using capacitors as admittance inverters,[17] we only need to control the length of each line, which supports straightforward design and fabrication. Note that using transmission line elements means there will be other passbands at integer multiples of ω_0 (see the supplementary material). Other ways to implement similar bandpass filters include smaller footprint mechanical resonators[21,38] and lumped-element LC resonators.[22,23,39] Some alternative circuit realizations are also shown in the supplementary material.

We experimentally implement a version of the circuit in Fig. 4, using a symmetric (zero insertion loss), 4th order filter. We couple four qubits via their readout resonators to the bandpass filter. Two readout resonators are coupled to the second stage and the other two to the third stage of the filter. The circuit diagram of this sample is shown in the supplementary material.

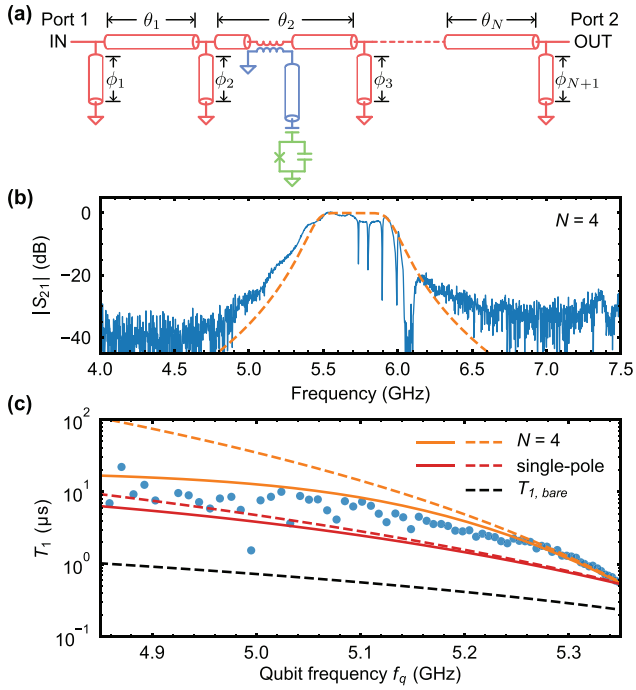

FIG. 4. Experimental realization. (a) Circuit diagram for an Nth order bandpass filter implemented using sections of transmission line in place of lumped-element LC resonators. (b) We experimentally implement a 4th order, zero insertion loss version of this circuit, coupling four qubits to the filter via their readout resonators, two connected to the second and two to the third filter stages. We measure the transmission $|S_{21}|$ of the qubit readout circuit, from input port (port 1) to output port (port 2); background attenuation is subtracted. There are four dips between 5.7 and 6.0 GHz, corresponding to each of the four qubit readout resonators. The broader dip at 6.1 GHz is due to the TWPA (see discussion). The orange dashed line is the coupled-mode simulation data for a symmetric 4th order bandpass filter with 5.7 GHz center frequency and 500 MHz bandwidth. (c) Qubit T_1 vs qubit frequency. The qubit is coupled to the 5.800 GHz readout resonator. Dashed lines are simulated qubit T_1 limit with a 4th order symmetric filter (orange), a single-pole bandpass filter (red) and without any filter (black). Solid lines are qubit T_1 limit including the intrinsic qubit loss ($T_1 = 20\ \mu$s) with a 4th order symmetric filter (orange) and a single-pole bandpass filter (red).

The circuit is fabricated on two separate sapphire substrates. The qubits and readout resonators are fabricated on one die, and the bandpass filter and control wiring on a separate die. An aluminum base layer is first deposited by electron beam evaporation, and the circuit pattern defined by reactive plasma etching through a photoresist stencil. The qubit Josephson junctions are liftoff deposited using the Dolan bridge method.[40] The two dies are then aligned and attached to one another using a flip-chip bonding technique.[41,42]

The assembly is wirebonded into a chip mount and cooled to 10 mK on the mixing chamber stage of a dilution refrigerator. The filter output signal is amplified by a traveling-wave parametric amplifier (TWPA)[43] at the 10 mK stage and a cryogenic HEMT amplifier at the 4 K stage. The transmission $|S_{21}|$ of the readout circuit, measured from

the input port (port 1) to the output port (port 2), is shown in Fig. 4(b). The bandpass filter is designed to have a center frequency $\omega_0/2\pi = 5.70$ GHz, bandwidth $\Delta\omega/2\pi = 500$ MHz, and maximally flat response. The frequencies of the four readout resonators are 5.736, 5.800, 5.896, and 5.993 GHz, as seen in the transmission data. These resonators have loaded quality factors Q_l around 500, corresponding to a dissipation rate $\kappa_r \approx 2\pi \times 12$ MHz. There are some ripples in the passband, which are possibly due to the flip-chip integration.[44]

We measured the qubit relaxation time T_1 vs qubit frequency f_q, where the qubit is tuned by applying a rectangular current pulse to its flux-bias coil during the measurement. The measured results are shown in Fig. 4(c). The experimental data (blue dots) at high frequencies agree well with simulation (orange dashed line) and are above the qubit T_1 limit with a single-pole bandpass filter[6] (red dashed line) and without the filter (black dashed line). The qubit lifetime at lower frequencies is shorter than the simulation results, which is limited by other loss mechanisms, e.g., dielectric loss, nonequilibrium quasiparticles, packaging, etc. If we consider the qubit intrinsic loss (i.e., T_1 is limited to 20 μs), the simulation data (orange solid line) agree better with the experimental data. Similar results were found for the other three qubits. We also demonstrate multiplexed qubit readout, with the results shown in the supplementary material. We also fabricated and measured a second-order asymmetric filter, whose transmission data are shown in the supplementary material.

We have characterized our device using transmission from the input to the output port. Another common method is to perform a reflection measurement from the input port. In our scheme, this can be realized by using a large insertion loss bandpass filter and measuring the reflection from the output port (setting κ_1 to zero as a singly terminated filter). We note that individual Purcell filters for each readout resonator can be added to suppress off-resonant driving.[14]

In summary, we present a systematic way to design and analyze broadband bandpass Purcell filters for circuit QED. We numerically show that large insertion loss filters can provide better qubit protection compared to conventional symmetrical filters. We experimentally implement these filters using a simple transmission line implementation and measure the performance for a 4th order symmetric filter implementation. This design can be easily integrated into existing superconducting quantum processor designs.

See the supplementary material for additional details for constructing bandpass filters with different insertion loss values as well as alternative circuit implementations, more detailed explanations of the coupled-mode theory and local density of states, and more details on the qubit experiments.

The authors want to thank Ofer Naaman for helpful and insightful comments. The authors also want to thank W. D. Oliver and G. Calusine at MIT Lincoln Lab for providing the traveling-wave parametric amplifier (TWPA) used in this work. This work was supported by the NSF QLCI for HQAN (NSF Award No. 2016136), the Air Force Office of Scientific Research, and in part based on work supported by the U.S. Department of Energy Office of Science National Quantum Information Science Research Centers and by UChicago's MRSEC (NSF Award No. DMR-2011854). We made use of the Pritzker Nanofabrication Facility, which receives support from SHyNE, a node of the National Science Foundation's National Nanotechnology Coordinated Infrastructure (NSF Grant No. NNCI ECCS-2025633).

AUTHOR DECLARATIONS

Conflict of Interest

The authors have no conflicts to disclose.

Author Contributions

Haoxiong Yan: Conceptualization (lead); Data curation (lead); Formal analysis (lead); Investigation (lead); Methodology (lead); Software (lead); Validation (lead); Visualization (lead); Writing – original draft (lead); Writing – review & editing (equal). **Xuntao Wu:** Formal analysis (equal); Investigation (lead); Methodology (supporting); Writing – review & editing (equal). **Andrew Lingenfelter:** Formal analysis (equal); Methodology (lead); Visualization (supporting); Writing – review & editing (equal). **Yash Joshi:** Investigation (supporting); Writing – review & editing (supporting). **Gustav Andersson:** Writing – review & editing (supporting). **Christopher R. Conner:** Writing – review & editing (supporting). **Ming-Han Chou:** Writing – review & editing (supporting). **Joel Grebel:** Writing – review & editing (supporting). **Jacob M. Miller:** Writing – review & editing (supporting). **Rhys Geoffrey Povey:** Writing – review & editing (supporting). **Hong Qiao:** Writing – review & editing (supporting). **Aashish Clerk:** Methodology (supporting); Writing – review & editing (equal). **Andrew N. Cleland:** Funding acquisition (lead); Supervision (lead); Writing – review & editing (lead).

DATA AVAILABILITY

The data that support the findings of this study are available from the corresponding author upon reasonable request.

REFERENCES

[1]A. Blais, A. L. Grimsmo, S. Girvin, and A. Wallraff, "Circuit quantum electrodynamics," Rev. Mod. Phys. **93**, 025005 (2021).
[2]A. Wallraff, D. I. Schuster, A. Blais, L. Frunzio, J. Majer, M. H. Devoret, S. M. Girvin, and R. J. Schoelkopf, "Approaching unit visibility for control of a superconducting qubit with dispersive readout," Phys. Rev. Lett. **95**, 060501 (2005).
[3]J. Koch, T. M. Yu, J. Gambetta, A. A. Houck, D. I. Schuster, J. Majer, A. Blais, M. H. Devoret, S. M. Girvin, and R. J. Schoelkopf, "Charge-insensitive qubit design derived from the Cooper pair box," Phys. Rev. A **76**, 042319 (2007).
[4]E. M. Purcell, "Spontaneous emission probabilities at radio frequencies," in *Confined Electrons and Photons* (Springer US, 1995) pp. 839–839.
[5]M. D. Reed, B. R. Johnson, A. A. Houck, L. DiCarlo, J. M. Chow, D. I. Schuster, L. Frunzio, and R. J. Schoelkopf, "Fast reset and suppressing spontaneous emission of a superconducting qubit," Appl. Phys. Lett. **96**, 203110 (2010).
[6]E. Jeffrey, D. Sank, J. Mutus, T. White, J. Kelly, R. Barends, Y. Chen, Z. Chen, B. Chiaro, A. Dunsworth, A. Megrant, P. O'Malley, C. Neill, P. Roushan, A. Vainsencher, J. Wenner, A. Cleland, and J. M. Martinis, "Fast accurate state measurement with superconducting qubits," Phys. Rev. Lett. **112**, 190504 (2014).
[7]D. T. Sank, "Fast, accurate state measurement in superconducting qubits," Ph.D. thesis (University of California, Santa Barbara, 2014).
[8]E. A. Sete, J. M. Martinis, and A. N. Korotkov, "Quantum theory of a bandpass Purcell filter for qubit readout," Phys. Rev. A **92**, 012325 (2015).
[9]T. Walter, P. Kurpiers, S. Gasparinetti, P. Magnard, A. Potočnik, Y. Salathé, M. Pechal, M. Mondal, M. Oppliger, C. Eichler, and A. Wallraff, "Rapid high-

fidelity single-shot dispersive readout of superconducting qubits," Phys. Rev. Appl. **7**, 054020 (2017).
[10]Y. Sunada, S. Kono, J. Ilves, S. Tamate, T. Sugiyama, Y. Tabuchi, and Y. Nakamura, "Fast readout and reset of a superconducting qubit coupled to a resonator with an intrinsic Purcell filter," Phys. Rev. Appl. **17**, 044016 (2022).
[11]L. Chen, H.-X. Li, Y. Lu, C. W. Warren, C. J. Križan, S. Kosen, M. Rommel, S. Ahmed, A. Osman, J. Biznárová, A. F. Roudsari, B. Lienhard, M. Caputo, K. Grigoras, L. Grönberg, J. Govenius, A. F. Kockum, P. Delsing, J. Bylander, and G. Tancredi, "Transmon qubit readout fidelity at the threshold for quantum error correction without a quantum-limited amplifier," npj Quantum Inf. **9**, 26 (2023).
[12]A. P. M. Place, L. V. H. Rodgers, P. Mundada, B. M. Smitham, M. Fitzpatrick, Z. Leng, A. Premkumar, J. Bryon, A. Vrajitoarea, S. Sussman, G. Cheng, T. Madhavan, H. K. Babla, X. H. Le, Y. Gang, B. Jäck, A. Gyenis, N. Yao, R. J. Cava, N. P. de Leon, and A. A. Houck, "New material platform for superconducting transmon qubits with coherence times exceeding 0.3 milliseconds," Nat. Commun. **12**, 1779 (2021).
[13]C. Wang, X. Li, H. Xu, Z. Li, J. Wang, Z. Yang, Z. Mi, X. Liang, T. Su, C. Yang, G. Wang, W. Wang, Y. Li, M. Chen, C. Li, K. Linghu, J. Han, Y. Zhang, Y. Feng, Y. Song, T. Ma, J. Zhang, R. Wang, P. Zhao, W. Liu, G. Xue, Y. Jin, and H. Yu, "Towards practical quantum computers: Transmon qubit with a lifetime approaching 0.5 milliseconds," npj Quantum Inf. **8**, 3 (2022).
[14]J. Heinsoo, C. K. Andersen, A. Remm, S. Krinner, T. Walter, Y. Salathé, S. Gasparinetti, J.-C. Besse, A. Potočnik, A. Wallraff, and C. Eichler, "Rapid high-fidelity multiplexed readout of superconducting qubits," Phys. Rev. Appl. **10**, 034040 (2018).
[15]B. Saxberg, A. Vrajitoarea, G. Roberts, M. G. Panetta, J. Simon, and D. I. Schuster, "Disorder-assisted assembly of strongly correlated fluids of light," Nature **612**, 435–441 (2022).
[16]G. Matthaei, E. M. T. Jones, and L. Young, *Microwave Filters, Impedance-Matching Networks, and Coupling Structures* (Artech House Publishers, 1980).
[17]D. M. Pozar, *Microwave Engineering* (Wiley, 2011).
[18]H. R. Mohebbi, O. Benningshof, I. Taminiau, G.-X. Miao, and D. Cory, "Superconducting coplanar interdigital filter with robust packaging," IEEE Trans. Appl. Supercond. **25**, 1500604 (2015).
[19]N. T. Bronn, Y. Liu, J. B. Hertzberg, A. D. Córcoles, A. A. Houck, J. M. Gambetta, and J. M. Chow, "Broadband filters for abatement of spontaneous emission in circuit quantum electrodynamics," Appl. Phys. Lett. **107**, 172601 (2015).
[20]Z. Li, T. Roy, D. R. Perez, K.-H. Lee, E. Kapit, and D. I. Schuster, "Autonomous error correction of a single logical qubit using two transmons," arXiv:2302.06707 [quant-ph]. (2023).
[21]A. Y. Cleland, M. Pechal, P.-J. C. Stas, C. J. Sarabalis, E. A. Wollack, and A. H. Safavi-Naeini, "Mechanical Purcell filters for microwave quantum machines," Appl. Phys. Lett. **115**, 263504 (2019).
[22]X. Zhang, E. Kim, D. K. Mark, S. Choi, and O. Painter, "A superconducting quantum simulator based on a photonic-bandgap metamaterial," Science **379**, 278–283 (2023).
[23]V. S. Ferreira, G. Kim, A. Butler, H. Pichler, and O. Painter, "Deterministic generation of multidimensional photonic cluster states with a single quantum emitter," arXiv:2206.10076 [quant-ph]. (2022).
[24]O. Naaman and J. Aumentado, "Synthesis of parametrically coupled networks," PRX Quantum **3**, 020201 (2022).
[25]Z. Wang, Z. Bao, Y. Wu, Y. Li, C. Ma, T. Cai, Y. Song, H. Zhang, and L. Duan, "Improved superconducting qubit state readout by path interference," Chin. Phys. Lett. **38**, 110303 (2021).
[26]T. Roy, S. Kundu, M. Chand, A. M. Vadiraj, A. Ranadive, N. Nehra, M. P. Patankar, J. Aumentado, A. A. Clerk, and R. Vijay, "Broadband parametric amplification with impedance engineering: Beyond the gain-bandwidth product," Appl. Phys. Lett. **107**, 262601 (2015).
[27]J. Grebel, A. Bienfait, É. Dumur, H.-S. Chang, M.-H. Chou, C. R. Conner, G. A. Peairs, R. G. Povey, Y. P. Zhong, and A. N. Cleland, "Flux-pumped impedance-engineered broadband Josephson parametric amplifier," Appl. Phys. Lett. **118**, 142601 (2021).
[28]T. White, A. Opremcak, G. Sterling, A. Korotkov, D. Sank, R. Acharya, M. Ansmann, F. Arute, K. Arya, J. C. Bardin, A. Bengtsson, A. Bourassa, J. Bovaird, L. Brill, B. B. Buckley, D. A. Buell, T. Burger, B. Burkett, N. Bushnell, Z. Chen, B. Chiaro, J. Cogan, R. Collins, A. L. Crook, B. Curtin, S. Demura, A. Dunsworth, C. Erickson, R. Fatemi, L. F. Burgos, E. Forati, B. Foxen, W. Giang, M. Giustina, A. G. Dau, M. C. Hamilton, S. D. Harrington, J. Hilton, M. Hoffmann, S. Hong, T. Huang, A. Huff, J. Iveland, E. Jeffrey, M. Kieferová, S. Kim, P. V. Klimov, F. Kostritsa, J. M. Kreikebaum, D. Landhuis, P. Laptev, L. Laws, K. Lee, B. J. Lester, A. Lill, W. Liu, A. Locharla, E. Lucero, T. McCourt, M. McEwen, X. Mi, K. C. Miao, S. Montazeri, A. Morvan, M. Neeley, C. Neill, A. Nersisyan, J. H. Ng, A. Nguyen, M. Nguyen, R. Potter, C. Quintana, P. Roushan, K. Sankaragomathi, K. J. Satzinger, C. Schuster, M. J. Shearn, A. Shorter, V. Shvarts, J. Skruzny, W. C. Smith, M. Szalay, A. Torres, B. W. K. Woo, Z. J. Yao, P. Yeh, J. Yoo, G. Young, N. Zhu, N. Zobrist, Y. Chen, A. Megrant, J. Kelly, and O. Naaman, "Readout of a quantum processor with high dynamic range Josephson parametric amplifiers," Appl. Phys. Lett. **122**, 014001 (2023).
[29]R. Kaufman, T. White, M. I. Dykman, A. Iorio, G. Stirling, S. Hong, A. Opremcak, A. Bengtsson, L. Faoro, J. C. Bardin, T. Burger, R. Gasca, and O. Naaman, "Josephson parametric amplifier with Chebyshev gain profile and high saturation," arXiv:2305.17816 [quant-ph]. (2023).
[30]M. A. Beck, M. Selvanayagam, A. Carniol, S. Cairns, and C. P. Mancini, "Wideband Josephson parametric isolator," arXiv:2212.08563 [quant-ph]. (2022).
[31]R. Kwende, T. White, and O. Naaman, "Josephson parametric circulator with same-frequency signal ports, 200 MHz bandwidth, and high dynamic range," Appl. Phys. Lett. **122**, 224001 (2023).
[32]W. A. Harrison, *Solid State Theory* (Courier Corporation, 1980).
[33]H. Bruus and K. Flensberg, *Many-Body Quantum Theory in Condensed Matter Physics* (Oxford University Press, 2004).
[34]A. A. Clerk, M. H. Devoret, S. M. Girvin, F. Marquardt, and R. J. Schoelkopf, "Introduction to quantum noise, measurement, and amplification," Rev. Mod. Phys. **82**, 1155–1208 (2010).
[35]R. Barends, J. Kelly, A. Megrant, D. Sank, E. Jeffrey, Y. Chen, Y. Yin, B. Chiaro, J. Mutus, C. Neill, P. O'Malley, P. Roushan, J. Wenner, T. C. White, A. N. Cleland, and J. M. Martinis, "Coherent Josephson qubit suitable for scalable quantum integrated circuits," Phys. Rev. Lett. **111**, 080502 (2013).
[36]A. Bienfait, K. J. Satzinger, Y. P. Zhong, H.-S. Chang, M.-H. Chou, C. R. Conner, É. Dumur, J. Grebel, G. A. Peairs, R. G. Povey, and A. N. Cleland, "Phonon-mediated quantum state transfer and remote qubit entanglement," Science **364**, 368–371 (2019).
[37]Y. Zhong, H.-S. Chang, A. Bienfait, É. Dumur, M.-H. Chou, C. R. Conner, J. Grebel, R. G. Povey, H. Yan, D. I. Schuster, and A. N. Cleland, "Deterministic multi-qubit entanglement in a quantum network," Nature **590**, 571–575 (2021).
[38]Y. Chu and S. Gröblacher, "A perspective on hybrid quantum opto- and electromechanical systems," Appl. Phys. Lett. **117**, 150503 (2020).
[39]M. Scigliuzzo, G. Calajò, F. Ciccarello, D. P. Lozano, A. Bengtsson, P. Scarlino, A. Wallraff, D. Chang, P. Delsing, and S. Gasparinetti, "Controlling atom-photon bound states in an array of Josephson-junction resonators," Phys. Rev. X **12**, 031036 (2022).
[40]G. J. Dolan, "Offset masks for lift-off photoprocessing," Appl. Phys. Lett. **31**, 337–339 (1977).
[41]K. J. Satzinger, C. R. Conner, A. Bienfait, H.-S. Chang, M.-H. Chou, A. Y. Cleland, É. Dumur, J. Grebel, G. A. Peairs, R. G. Povey, S. J. Whiteley, Y. P. Zhong, D. D. Awschalom, D. I. Schuster, and A. N. Cleland, "Simple non-galvanic flip-chip integration method for hybrid quantum systems," Appl. Phys. Lett. **114**, 173501 (2019).
[42]C. R. Conner, A. Bienfait, H.-S. Chang, M.-H. Chou, É. Dumur, J. Grebel, G. A. Peairs, R. G. Povey, H. Yan, Y. P. Zhong, and A. N. Cleland, "Superconducting qubits in a flip-chip architecture," Appl. Phys. Lett. **118**, 232602 (2021).
[43]C. Macklin, K. O'Brien, D. Hover, M. E. Schwartz, V. Bolkhovsky, X. Zhang, W. D. Oliver, and I. Siddiqi, "A near–quantum-limited Josephson traveling-wave parametric amplifier," Science **350**, 307–310 (2015).
[44]H.-X. Li, D. Shiri, S. Kosen, M. Rommel, L. Chayanum, A. Nylander, R. Rehammer, G. Tancredi, M. Caputo, K. Grigoras, L. Grönberg, J. Govenius, and J. Bylander, "Experimentally verified, fast analytic, and numerical design of superconducting resonators in flip-chip architectures," IEEE Trans. Quantum Eng. **4**, 3101312 (2023).